

Imaging of the Peripheral Nervous System: Evaluation of Peripheral Neuropathy and Plexopathy

Kenneth R. Maravilla and Brian C. Bowen

Over the past decade, technical advances in MR imaging of the CNS have resulted in improved diagnosis and evaluation of encephalopathy, myelopathy, and cranial neuropathy. Parallel advances in imaging of the peripheral nervous system have not occurred, and the evaluation of peripheral neuropathy or plexopathy has relied principally on the patient's clinical history and the neurologic examination, with relatively few requests for imaging studies. Routine CT and MR imaging have been useful to exclude mass lesions in the vicinity of a peripheral nerve, but there has not been an effective method for directly imaging the nerve (1, 2).

Also, in the last decade, neurologic and orthopedic surgeons have become skilled in newer, more sophisticated microsurgical procedures to repair damaged nerves, and many of these surgeons have chosen to specialize in peripheral nerve treatment. For these reasons, noninvasive techniques are needed that improve the diagnostic accuracy of peripheral neuropathy and facilitate preoperative planning when surgery is contemplated. Currently, electrophysiological studies are widely used and have high sensitivity for detecting a conduction abnormality; however, they lack specificity and cannot display the anatomic detail needed for precise localization and treatment planning. High-resolution imaging of peripheral nerves potentially overcomes these limitations and, consequently, recent interest has focused on improved MR imaging techniques that use phased-array radiofrequency (RF) coil technology and rapid acquisition of imaging data (3–5).

Anatomy

Peripheral Nerves

The basic unit of the peripheral nerve is the axon, which may be myelinated or unmyelinated, and carry efferent (motor) or afferent (sensory) electrical impulses. Isolated peripheral nerves in the extremities, as well as nerves composing the brachial and lumbosacral plexus, are a mixture of such axons. Myelinated axons are enclosed by many layers of compacted Schwann cell membranes, which form the myelin

sheath, whereas “unmyelinated” axons merely invaginate into grooves in the Schwann cell cytoplasm. The fluid-containing periaxonal space between the axon membrane and the apposed Schwann cell membrane is less than 20 nm wide. For both myelinated and unmyelinated axons, there is a basement membrane (or basal lamina) that surrounds the external surface of the Schwann cell–axon complex.

The largest peripheral nerves have three connective tissue sheaths that support and protect the complex (6). The innermost sheath is the endoneurium. It consists of loose vascular connective tissue and extracellular fluid. The endoneurium invests the Schwann cell–axon complex. Its inner border is thus the Schwann cell basement membrane, and its outer border is the second connective tissue sheath, the perineurium. The axons, Schwann cells, and endoneurium are bundled together into fascicles, each of which is encompassed by a dense perineurial sheath (Fig 1). The endoneurial fluid within each fascicle is isolated from the general extracellular space by tightly adherent epithelial-like cells of the perineurium and from the circulating blood by the tight junctions between endothelial cells of the endoneurial capillaries. The perineurium acts as a protective barrier to infectious or toxic agents; however, once this barrier is penetrated, there is the potential for spread of disease along the fascicle.

The epineurium is the outermost connective tissue sheath. It envelops the nerve and has extensions that encompass each of the perineurial-lined fascicles, providing mechanical support for the axons when they are subjected to stretching forces. The epineurium consists of dense, irregular connective tissue, with thick collagen and elastin fibers. Variable amounts of interfascicular adipose tissue are present within the larger nerves (Fig 1). For example, the sciatic nerve contains appreciable quantities of fat, whereas the nerves of the upper limb have relatively little fat (7). Nutrient vessels penetrate the nerve at frequent intervals along its course, communicating with the longitudinally oriented epineurial, interfascicular, perineurial, and intrafascicular arteries and arterioles. At the central or proximal end of the spinal

Supported in part by a Dana Foundation Grant for Clinical Hypotheses in the Neurological Sciences (K.R.M.).

From the Departments of Radiology and Neurological Surgery, University of Washington, Seattle, WA (K.R.M.); and the Departments of Radiology and Neurological Surgery, University of Miami School of Medicine, Miami, FL (B.C.B.).

Address reprint requests to Kenneth R. Maravilla, MD, Department of Radiology, University of Washington, Box 357115, Seattle, WA 98195.

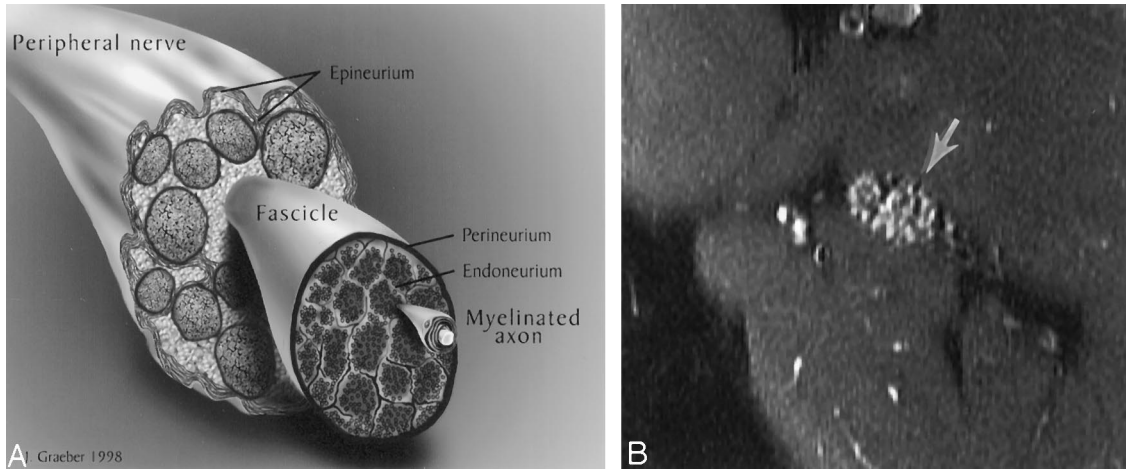


FIG 1. A, Schematic drawing of peripheral nerve anatomy. Fascicles within large peripheral nerves are interspersed with variable amounts of adipose tissue and surrounded by epineurium. Each fascicle (*enlarged segment*) is enclosed by a ring of dense perineurium and contains myelinated and unmyelinated axons supported by loose endoneurial connective tissue. B, Axial fat-suppressed T2-weighted (5000/102/2; echo train length = 8) MR image of a sciatic nerve (*arrow*) shows the same fascicular pattern illustrated in A. The fascicles display a honeycomblike appearance of hyperintense signal interspersed with adipose tissue and connective tissue, which appear dark.

nerves, the epineurium is continuous with the dura mater. At the distal or peripheral end of the peripheral nerves, the epineurium is progressively reduced in thickness, eventually being incorporated into the perineurium.

The largest peripheral nerves are approximately 1 to 10 mm in diameter (up to 20 mm for the sciatic nerve), and contain on the order of 10 fascicles (range, 1 to 100) (7). Each fascicle is usually composed of motor, sensory, and sympathetic fibers. The number and size of fascicles vary from nerve to nerve and along the length of any single nerve. The longitudinal variation occurs because fascicles repeatedly unite and divide along the course of the nerve, allowing the passage of axons from one fascicle to another. Sunderland (7) has reported that the largest fascicles in formalin-fixed nerves are 3.5 mm in diameter, while the smallest are about 0.05 mm. He also identified the average number of fascicles and the percentage of cross-sectional area of the nerve occupied by them at different locations along the median, ulnar, and radial nerves, as well as in the tibial and common peroneal divisions of the sciatic nerve.

As indicated in Figure 1B, MR imaging can depict fascicles on high-resolution sequences *in vivo*. The MR signal characteristics of normal, large peripheral nerves have been described in previous reports (3–5) and have recently been verified by Ikeda et al (8) in a study comparing MR imaging findings in cadavers with histopathologic specimens. The clustered dotlike structures seen on high-resolution, cross-sectional MR images represent the fascicles, and it has been suggested that their signal characteristics are due to endoneurial fluid (4, 5, 9).

Neural Plexus

Proper interpretation of MR imaging studies of the nerves requires a detailed knowledge of the regional

anatomy of the neural plexus and/or isolated peripheral nerves of interest, as well as the location of the muscle(s) innervated by the nerve(s). This knowledge helps to locate the site of abnormality of the nerve in question and to avoid pitfalls in nerve identification. Incorrect identification of a nerve can occur either by mistaking one nerve for another, where two or more nerves run in proximity, or by mistaking a linear structure, such as a small blood vessel, tendon, or muscular bundle, for a nerve.

The brachial and lumbosacral plexus are networks of peripheral nerves, and thus the components of each network have the basic endoneurium-perineurium-epineurium organization and fascicular structure described above for an isolated peripheral nerve. A component nerve can be identified on MR nerve images if the observer is familiar with the intrinsic anatomy of the plexus and the relationship of the component of interest to adjacent muscles, vessels, and osseous landmarks.

Each plexus is formed from the ventral rami of a set of spinal nerves. The brachial plexus is formed from the ventral rami of the C5–T1 spinal nerves. The ventral rami are the *roots* of the plexus. They form the upper, middle, and lower *trunks* in or near the cleft between the anterior and middle scalene muscles, known as the interscalene triangle (1) (plane A in Fig 2; Fig 3A–D). More laterally, the trunks divide into anterior and posterior *divisions* just distal to the interscalene triangle (plane B in Fig 2; Fig 3E and F). Subsequently, these divisions join to form three *cords* distal to the lateral margin of the first rib (sagittal plane C in Fig 2). The subclavian artery travels through the interscalene triangle with the plexus while the subclavian vein courses anterior to the anterior scalene muscle. In the axilla, the neurovascular complex within the axillary sheath consists of the axillary artery, the adjacent lateral, posterior, and medial cords, and the axillary vein. At sagittal plane C

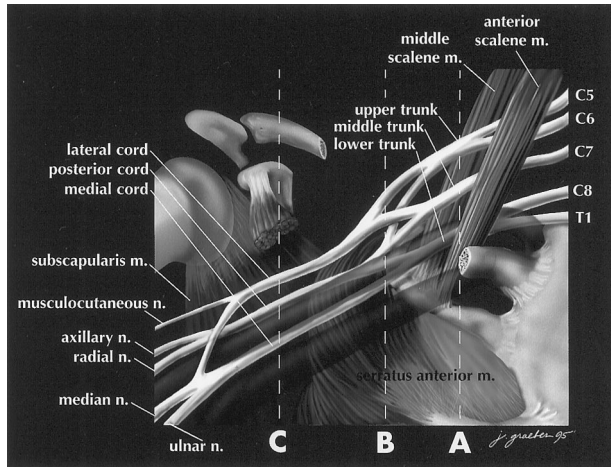


FIG 2. Schematic representation of brachial plexus: The C5–T1 ventral rami are called roots. These form three trunks near the anterolateral margins of the anterior and middle scalene muscles (interscalene triangle, plane A). The trunks divide into anterior and posterior divisions more laterally, and then join to form the three cords near the lateral margin of the first rib (plane B). The subclavian artery travels through the interscalene triangle with the plexus, while the subclavian vein courses anterior to the anterior scalene muscle. In the axilla, the neurovascular complex consists of the axillary artery and vein and the cords of the plexus. At plane B, the complex is bordered anteriorly by the pectoralis major muscle and posteriorly by the serratus anterior muscle. At plane C (approximate level of coracoid process), the anterior and posterior borders are the pectoralis minor and the subscapularis muscles, respectively. Each cord ends in two terminal branches. Reprinted with permission from (1).

(coracoid process), the anterior and posterior borders are the pectoralis minor and the subscapularis muscles, respectively. Each cord ends in two major terminal branches.

The lumbosacral plexus consists of two separate plexus, the lumbar and the sacral (2) (Fig 4). The lumbar plexus is formed from the L1–L3 ventral rami, with contributions from T12 and L4. The rami, or roots, divide into anterior and posterior divisions. The anterior divisions combine to form the anterior branches (iliohypogastric, ilioinguinal, genitofemoral, and obturator nerves) of the plexus, and the posterior divisions combine to form the posterior branches (femoral and lateral femoral cutaneous nerves) within the psoas major muscle. The anterior and posterior branches are distributed to the embryonic anterior (ventral) and posterior (dorsal) skin and musculature of the lower limb, respectively. In the adult, the anteroposterior relationships are altered primarily because of the medial rotation that the lower limb undergoes during development. Thus, the femoral nerve, which is a posterior branch of the plexus, innervates muscles and skin on the front of the thigh (sartorius, quadriceps) and skin on the medial aspect of the thigh and leg (saphenous branch of femoral nerve). In general, the lumbar plexus innervates the muscles of the anterior and medial thigh while the sacral plexus innervates the muscles of the buttock and posterior thigh and all those below the knee.

The sacral plexus is formed from the ventral rami of L4–L5 (lumbosacral trunk) and S1–S4. Again, an-

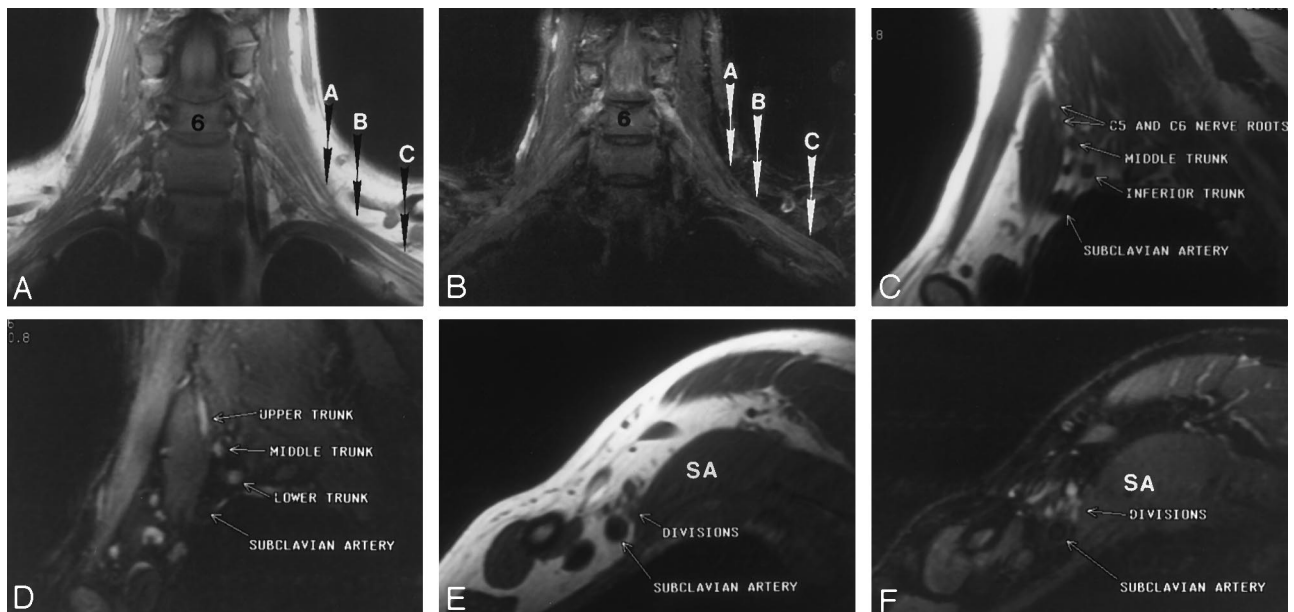


FIG 3. MR images of the brachial plexus.

A and B, Coronal T1-weighted (600/10/2) (A) and STIR (4000/34/160/2; echo train length = 4) (B) images of the brachial plexus show the major nerve roots originating from the cervical spine that subsequently join to form trunks within the interscalene triangle (A). These continue distally to form divisions (B) and then subsequently cords (C).

C and D, Sagittal images at the level of the interscalene triangle (roughly corresponding to the plane denoted A in A and B) show the C5 and C6 nerve roots as they come together to form the upper trunk as well as the middle and lower trunks within the interscalene triangle. Note the position of these trunks superior to the subclavian artery.

E and F, Sagittal images at a plane approximately corresponding to that labeled by B in A and B. At this level, the divisions of the brachial plexus can be seen. Note their position forming a triangle-like configuration just above the subclavian artery. The posterior margin of the brachial plexus divisions is bordered by the serratus anterior muscle (SA).

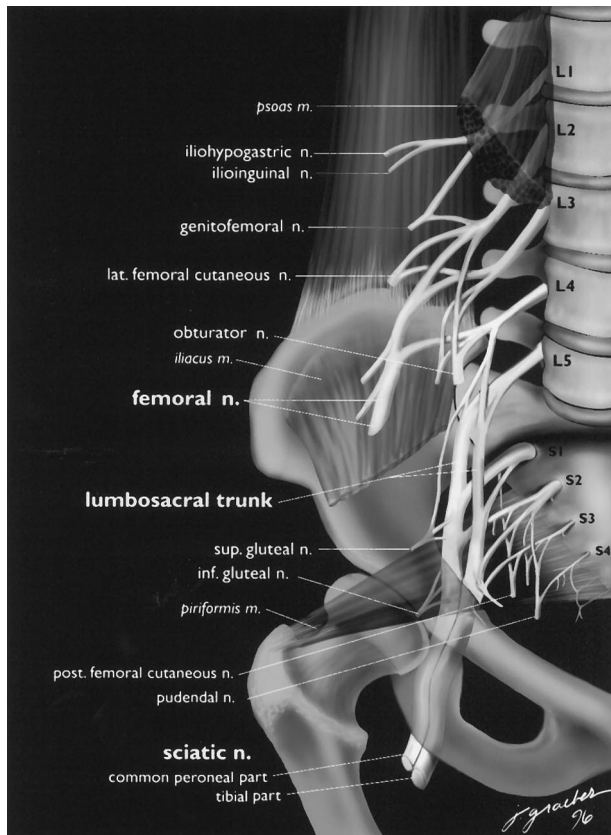


FIG 4. Schematic representation of lumbar and sacral plexus: the lumbar plexus is formed from the L1–L3 ventral rami, with contributions from T12 and L4. The sacral plexus is formed from the ventral rami of L4, L5 (lumbosacral trunk), and S1–S4. The sciatic nerve (L4–S3) exits the pelvis through the greater sciatic foramen ventral to the piriformis muscle. The common peroneal and tibial branches of the sciatic nerve separate in the lower thigh. Anterior divisions of the rami forming the sacral plexus give rise to the tibial part of the sciatic nerve, while posterior divisions give rise to the common peroneal part of sciatic nerve. Reprinted with permission from (2).

terior and posterior divisions give rise to anterior and posterior branches. The anterior branches include the tibial part of the sciatic nerve, pudendal nerve, and medial part of the posterior femoral cutaneous nerve, whereas the posterior branches include the common peroneal part of sciatic nerve, superior and inferior gluteal nerves, lateral part of the posterior femoral cutaneous nerve, and the nerve to the piriformis muscle. Located anterior to the piriformis muscle and the sacroiliac joint, the sacral plexus is a broad triangular network whose apex is the sciatic nerve (Fig 4; Fig 5). The sciatic nerve (L4–S3) exits the pelvis through the greater sciatic foramen along with the piriformis muscle and the superior and inferior gluteal vessels and nerves. The sciatic nerve courses laterally in the gluteal region, approaches the middle, posterior portion of the upper thigh, and then continues inferiorly until dividing into the common peroneal and tibial nerves in the region of the lower third of the femur.

The internal iliac vessels are located anteromedial to the lumbosacral trunk at the level of the sacral promontory. The superior gluteal branches pass be-

tween the lumbosacral trunk and S1 (or between S1 and S2), turning laterally immediately inferior to the sacroiliac joint and exiting the pelvis along with the superior gluteal nerve. The inferior gluteal vessels usually pass between S1 and S2 or between S2 and S3. These vessels lie posteromedial to the sciatic nerve and accompany it through the greater sciatic foramen. The internal pudendal vessels are located between the ischial part of the spine and the pudendal nerve and follow its course through the greater and lesser sciatic foramina.

Methods

RF Coils

To obtain highly detailed images of peripheral nerves, specialized RF receiver coils are used. Although one of the authors has used custom-designed phased-array coils exclusively, commercially produced surface coils can be substituted and can produce adequate images. Each set of custom phased-array coils is specifically designed to optimize imaging of a specific body region. Phased-array RF coil technology integrates signal data from multiple small coils to produce a single image, mimicking a single larger coil. The RF signal from each small coil is collected independently of the other coils in the phased array, and each contributes signal from a small field-of-view (FOV) with high signal-to-noise ratio (SNR). By combining the signals from the multiple small coils, an image can be produced that has the high SNR of each small coil yet encompasses a composite FOV similar to that of a single larger surface coil (10, 11). In addition to these advantages, the phased-array assembly is flexible and can be shaped to fit the curved contours of the body in regions such as the side of the neck and the supraclavicular area (12). The image produced from the phased-array configuration is thus markedly improved relative to the image produced by using a single larger surface coil or a whole-body coil. Because only a relatively small FOV can be imaged with high spatial resolution, it is necessary to clinically establish the site of a suspected neuropathic lesion as accurately as possible before the MR study.

Pulse Sequences and Fat Suppression

Evaluation of the peripheral nervous system, like that of the CNS, involves the acquisition of flow-compensated, T1- and T2-weighted images. Standard spin-echo sequences are used to generate the T1-weighted images. These images display regional anatomy, including the various muscles, blood vessels, and nerves outlined by tissue fat planes.

Fast spin-echo sequences are used to generate the T2-weighted images. These images help to detect pathologic signal changes within a nerve; however, since nerves are small, the abnormal signal within a nerve is easily obscured by signal from surrounding fat. To overcome this problem, various methods of fat suppression are used in conjunction with the fast spin-echo sequence. The two most common methods

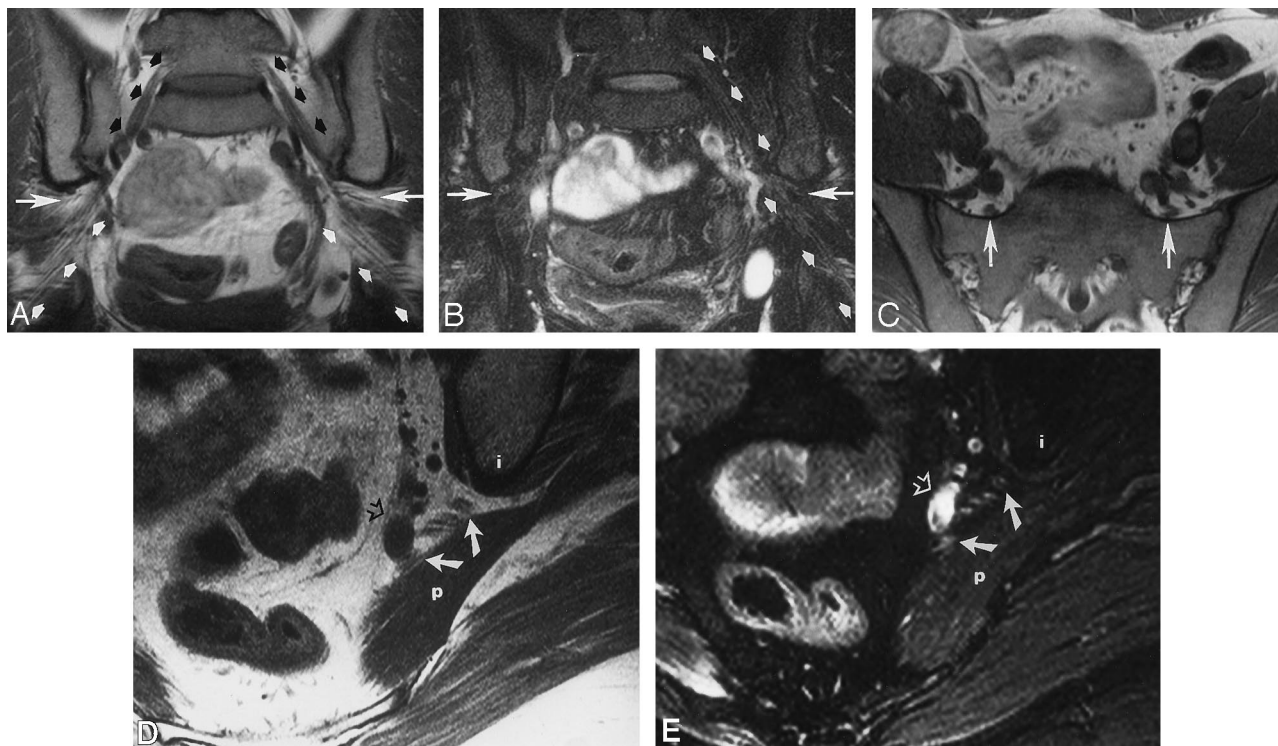


FIG 5. MR imaging appearance of the normal sacral plexus.

A and B, Coronal T1-weighted (A) and STIR (B) images of the normal sacral plexus show the course of the lumbosacral trunk (*upper three arrows*) as these nerves course obliquely inferiorly and laterally, anterior to the sacral wings within the pelvis. They then exit the pelvis through the greater sciatic foramen (*long white arrows*) as the sciatic nerve (*lower three arrows*). Note the linear striated appearance of the nerves on both the T1-weighted and STIR images, which is believed to reflect the individual nerve fascicles constituting the lumbosacral trunk and sciatic nerves.

C, Axial T1-weighted image at the level of the sacral wings shows the lumbosacral trunks as they course anterior to these structures (*arrows*).

D, Axial T1-weighted image at the level of the greater sciatic foramen shows the left sacral plexus components (lumbosacral trunk and S1–S3) as clustered linear segments (*closed arrows*) anterior to the piriformis muscle (p), posterior to the ischium (i), and lateral to the inferior gluteal vessels (*open arrow*). Slightly inferior to this section, the obliquely oriented components come together to form the sciatic nerve, which exits the pelvis through the greater sciatic foramen.

E, Corresponding fast spin-echo T2-weighted image with fat suppression shows the normal slight hyperintensity of the plexus components.

are frequency-selective saturation of the fat resonance and short-inversion-time inversion recovery (STIR) with nulling of the signal contribution from fat. Each method has its advantages and disadvantages.

In general, the STIR method has proved to be more reliable, since it provides uniform and consistent suppression of fat signal from patient to patient while maintaining excellent T2 contrast. There are, however, two disadvantages to the STIR method. The first is relatively low SNR. The second is greater sensitivity to blood-flow artifacts. Consequently, flow saturation bands are used in an attempt to eliminate, or to greatly attenuate, these phase shift-artifacts that degrade the resulting STIR image.

The frequency-selective fat-saturation method has higher SNR and fewer blood-flow related artifacts; however, the major disadvantage of this method is inhomogeneous fat suppression across the FOV. The variable fat suppression is mainly due to field inhomogeneity caused by variation in magnetic susceptibility differences across the body. Because of these effects, T2-weighted (or T1-weighted) images may

contain some areas with incomplete suppression or “bleed-through” of fat signal as well as other areas with suppression of the water signal rather than the fat signal. This results in poor visualization of nerves and sometimes of adjacent anatomic landmarks. The observed inhomogeneity of fat saturation may be further accentuated by nonuniformity in signal reception of the surface coils. Because of the difficulty in overcoming bulk susceptibility artifacts (13), especially in areas with high susceptibility differences, such as the base of the neck, or when imaging a larger FOV, the STIR method is preferred for T2-weighted imaging at this time.

Image Orientation and FOV

Whenever possible, images are obtained in at least two planes. Usually, images approximately parallel to (in-plane images) and perpendicular to (cross-sectional images) the long axis of the nerve are obtained. The in-plane images show the long axis of the nerve, allowing one to scrutinize the course of the nerve for displacement or focal enlargement. These images,

however, suffer from partial-volume artifacts, which can result in inaccurate assessment of signal intensity within a nerve on T2-weighted acquisitions. Cross-sectional images, on the other hand, avoid this partial-volume problem and allow assessment of the relative size and cross-sectional shape of the nerve. Images obtained perpendicular to the nerve also allow better assessment of the fascicular pattern, and focal areas of expansion or compression can still be evaluated on cross-sectional nerve images by comparing successive sections.

Brachial and Sacral Plexus

In the evaluation of the brachial plexus, image orientation parallel to the sagittal plane of the body may be preferred by some investigators to true cross-sectional views of the plexus, because anatomic landmarks are identified more easily with the sagittal orientation (Fig 3C–F). True sagittal images, though, are not perpendicular to the axis of plexus components, such as the cords, and this can cause occasional difficulty with identification and evaluation of these components. An alternative approach is to use oblique sagittal images, which are more nearly perpendicular to the plexus components, for cross-sectional evaluation of the brachial plexus. In addition, axial images can be used to evaluate the sacral plexus. The FOV for imaging the brachial and sacral plexus is 24 to 26 cm, and a 512×256 or 512×512 matrix is used. Section thickness is 4 mm with contiguous images in the coronal plane and a gap of 50% to 100% (2 to 4 mm) in the cross-sectional plane of nerve imaging (sagittal brachial plexus or axial sacral plexus) to obtain sufficient length of coverage.

Peripheral Nerves

A complete description of the technical parameters involved in imaging all peripheral nerves is beyond the scope of this discussion; however, we can offer some general guidelines for performing these studies. T1- and T2-weighted images of a nerve are obtained in precisely the same plane and location and with a similar FOV so that the images are directly comparable. This congruity is necessary because the fat-suppressed T2-weighted images usually will not adequately show normal tissue planes (usually outlined by fat) and anatomic landmarks. Thus, the radiologist must rely on a comparison of the T1- and T2-weighted images to identify and spatially locate a nerve or critical landmarks. The FOV that is used depends on which area of the body is to be imaged. The FOV ranges from approximately 10 to 12 cm when examining small body parts, such as the wrist (for example, in patients with carpal tunnel compressive neuropathy) to approximately 14 to 16 cm when examining larger body areas, such as nerves in the upper arm or the sciatic nerve in the thigh. High spatial resolution is achieved by using as large a data matrix as possible while still maintaining adequate SNR. Matrix size ranges from 256×256 for the

smaller FOV to 512×256 or 512×512 for larger FOVs. Section thickness is between 3 and 4 mm. For small regions of interest, contiguous sections are obtained. For larger regions of interest, such as the sciatic nerve in the thigh, only the in-plane views are contiguous, whereas cross-sectional views (axial plane) often have a 50% to 100% gap (2 to 4 mm) between sections. The use of such a gap when imaging the nerve in cross section permits greater length of coverage of a peripheral nerve in a reasonable scan time.

Contrast Media

At present, there is limited utility for gadolinium-based intravenous contrast material in peripheral nerve imaging. For most cases, including traumatic nerve injury, compressive neuropathy, or unexplained neuropathy, a noncontrast examination is sufficient. Nevertheless, contrast material has proved useful for a few indications, such as in examinations of patients with suspected neoplasm, inflammation, or abscess formation, and in postoperative evaluations. A standard dose of 0.1 mmol/kg is used and is administered as an intravenous bolus. T1-weighted spin-echo images, with frequency-selective fat saturation, are acquired within 3 to 5 minutes after injection. As an alternative, out-of-phase T1-weighted spoiled gradient-echo imaging appears promising, because it shows more homogeneous fat suppression (Maravilla KR, unpublished results).

Imaging Appearance

Normal Nerves

The techniques outlined above provide reliable images of peripheral nerves measuring at least 2 to 3 mm in diameter. These include the following: nerves of the brachial and sacral plexus; the ulnar, median, and radial nerves in the arm and forearm; the median and ulnar nerves in the wrist; the sciatic nerve in the thigh; and the proximal tibial and peroneal nerves in the thigh, popliteal fossa, and leg (4, 5). MR evaluation of peripheral nerves is performed in two ways. The first and most important way is by direct high-resolution imaging of the nerve. The second way is by imaging the major muscle groups innervated by the nerve, looking for changes in signal intensity indicative of denervation (14–16).

T1-weighted images show the size and location of the nerve. In some cases, all or part of the course of the nerve may be obscured by surrounding muscle tissue, because of a lack of intervening fat. In these cases, comparison of T1- and T2-weighted images is done to trace the course of the nerve and to monitor its appearance. The normal nerve is oval or round. The size of a particular nerve, such as a sciatic or median nerve, varies along its length and from person to person. Corresponding normal nerves on the two sides of the body in the same person and at the same level, though, are of similar size. The rodlike fascicles within the nerve are visible on high-resolution, cross-

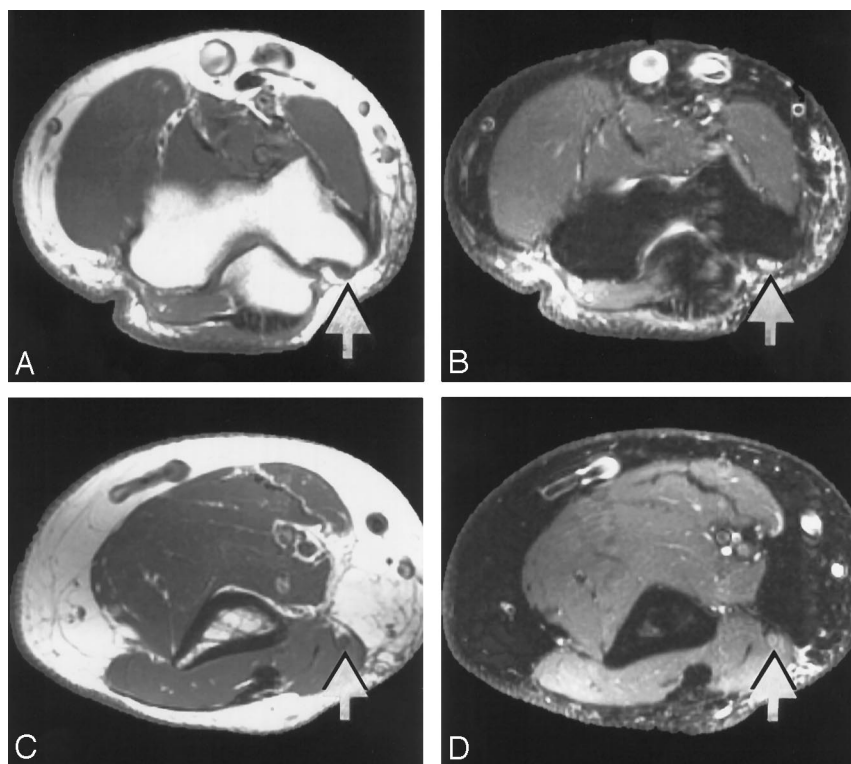


FIG 6. Patient with right ulnar neuropathy caused by entrapment in the cubital tunnel posterior to the medial epicondyle of the humerus.

A and B, T1-weighted (A) and STIR (B) images at the level of the cubital tunnel show normal-sized ulnar nerve (arrows). Note the fascicular appearance on B. The marked hyperintense T2 signal relative to muscle on this image is abnormal and is seen with various types of neuropathy.

C and D, T1-weighted (C) and STIR (D) images just proximal to the cubital tunnel show normal-appearing ulnar nerve. Note that the signal intensity on the STIR image is nearly isointense with adjacent muscle as compared with the abnormally increased signal present in B. The nerve also displayed normal signal intensity just distal to the cubital tunnel (*not shown*). This localized abnormal signal change within a nerve is common with entrapment syndromes, such as those that occur in the cubital or carpal tunnels. This figure also illustrates the importance of obtaining aligned T1- and T2-weighted images to unequivocally define the nerve that might otherwise be confused with a muscle, tendon, or blood vessel.

sectional images (Fig 1). Seen on end, the collection of fascicles within the nerve has a honeycomblike appearance, called a fascicular pattern (4, 5, 8). The fascicles appear uniform in size and generally mildly hyperintense relative to adjacent muscle on T2-weighted images (Fig 1B).

Comparison between T1-weighted images and fat-suppressed fast spin-echo or STIR T2-weighted images helps to confirm the size and location of the nerve. On T2-weighted images, the fascicles within a normal nerve are mildly hyperintense relative to adjacent muscle tissue. The intensity seems to vary slightly among nerves, with centrally located, larger nerves having a higher nerve/muscle signal intensity ratio than more peripheral, smaller nerves. For in-plane sections of a particular nerve, the signal intensity of the nerve is generally uniform in appearance throughout its length within the FOV. In cross section, the fascicular pattern is more easily discernible on T2-weighted images than on corresponding T1-weighted images.

Abnormal Nerves

Although the loss of fat planes around part or all of a nerve on T1-weighted images is often an abnormal finding associated with infiltrating or compressive lesions, this appearance may be normal in younger, thinner patients, who have a low percentage of body fat. Diffuse or focal enlargement of a nerve, though, is definitely abnormal, as is diffuse or focal marked hyperintensity on T2-weighted images. The assessment of differences in signal intensity is made by visual inspection and is therefore subjective. At

present, no reliable quantitative method for evaluating the signal intensity of normal versus abnormal nerves has been developed.

In some compressive neuropathies, focal hyperintense areas are observed in the affected nerve at the site of compression, while normal or nearly normal T2 signal intensity is present proximally and distally (5, 17, 18). Examples include compression of the ulnar nerve in the cubital tunnel (Fig 6) and compression of the median nerve in the carpal tunnel. The exact pathogenesis of this focal change in signal intensity is not known, but it may represent localized edema or increased fluid accumulation within the endoneurial spaces at the site of compression.

An altered fascicular pattern is another finding indicative of an abnormal nerve. In some cases, individual fascicles are not resolved even though the MR images are of sufficient quality to do so. In other cases, some fascicles are markedly enlarged and/or hyperintense relative to adjacent fascicles, resulting in a decidedly nonuniform pattern (Fig 7). In general, changes in the fascicular pattern are almost always accompanied by a marked increase in signal intensity within the abnormal nerve on T2-weighted images.

Indications for MR Imaging of the Nerves

The indications for MR imaging of the nerves (3–5, 9, 17–19) are evolving in response to continual improvements in MR imaging techniques and in methods for treating peripheral neuropathy. Current indications include those listed below.

FIG 7. Axial T1-weighted (A) and STIR (B) images through the midportion of the thigh show the appearance of an abnormal sciatic nerve (arrows). The sciatic nerve is markedly enlarged to approximately three to four times its normal size. The fascicular pattern is accentuated with marked heterogeneity in the size of the various fascicles, many of which are also grossly enlarged. Finally, there is marked hyperintense signal within the nerve relative to surrounding muscle on the STIR image. Complete evaluation of the nerve in this patient revealed that the enlargement, the abnormal fascicular pattern, and the abnormal hyperintensity were present throughout the entire length of the sciatic nerve from the pelvis to the knee. The pathogenesis was not proved, but a hypertrophic neuropathy or an inflammatory pseudotumor involving the nerve was suspected. The patient refused biopsy.

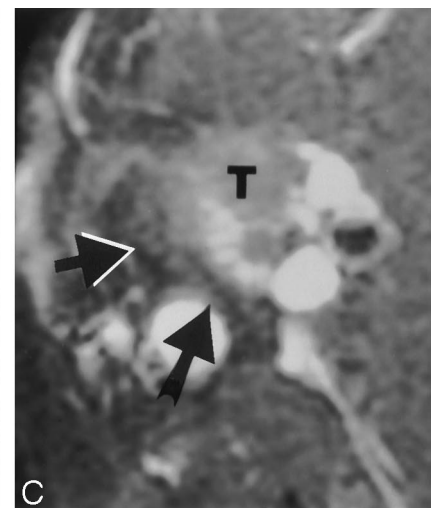
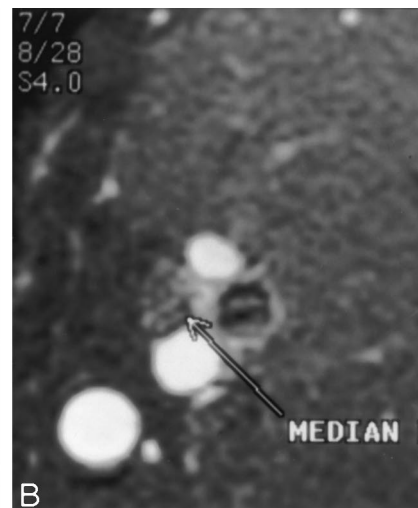
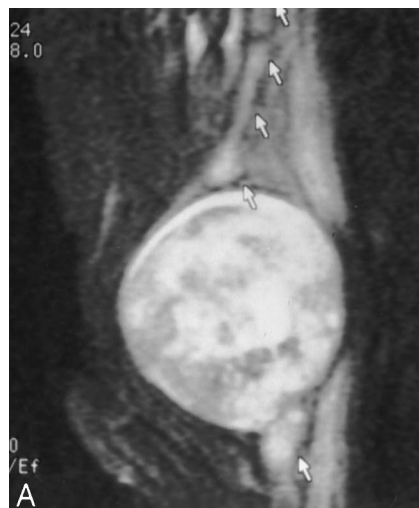
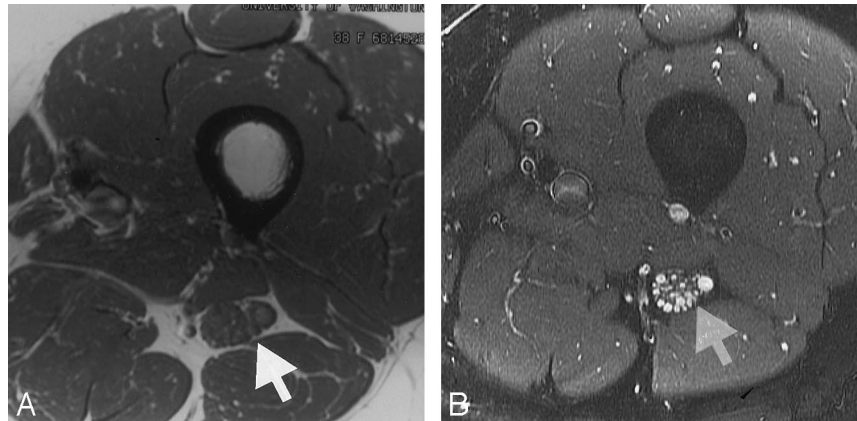


FIG 8. MR images of schwannoma of the median nerve in the upper arm show the extrinsic appearance of the tumor relative to the nerve fascicles, which are compressed and displaced around the periphery of the tumor.

A, Coronal fat-suppressed T2-weighted fast spin-echo image through the mass shows the displaced course and distorted appearance of the median nerve (arrows).

B and C, Axial T2-weighted images of the median nerve just proximal to the upper margin of the tumor (B) and at the level of the upper third of the tumor (T) (C) show the median nerve fascicles as they begin to spread apart just above the tumor (B). They then splay out in a linear fashion along the edge of the tumor (arrows, C). The nerve fascicles continued like this throughout the length of the tumor until they could be seen to come together again just inferior to the tumor. This appearance helps to clarify the extrinsic origin of the mass as well as to define the location of residual nerve fascicles for the surgeon preoperatively. The location of the nerve fascicles (which were functional) and the extrinsic origin of the tumor were both proved at surgical resection.

Mass Involving a Peripheral Nerve

MR imaging can often show whether a mass is intrinsic or extrinsic to a nerve and, if extrinsic, allow the physician to ascertain the site of the displaced and compressed nerve fibers before surgical intervention. This can aid in preoperative planning and help to shorten the surgical procedure (3, 5, 9) (Fig 8). This information is valuable in the diagnosis and management of patients with brachial or lumbosacral plexopathy due to neoplastic processes, such as nerve sheath tumors, metastases, direct extension of non-neural primary tumor, and lymphoma, or to benign processes, such as aggressive fibromatosis (desmoid tumor) or endometriosis. MR imaging has also proved useful in the detection of malignant primary or recurrent tumors infiltrating nerve structures, and has been especially helpful in cases in which clinical

examination and routine imaging studies were not able to distinguish whether a patient's symptoms were due to recurrent tumor, to postoperative or posttreatment changes due to scarring, or to a compressive neuropathy due to regional deformity (Fig 9).

Compressive Neuropathy and Nerve Entrapment Syndromes

Guided to the location of entrapment by the clinical and neurologic examination, MR imaging is used to detect objective imaging findings of nerve compression (20). Some of the peripheral nerves that are affected and the sites of entrapment include the median nerve in the carpal tunnel (3, 21), the ulnar nerve in the cubital tunnel (18, 22) (Fig 6) or in Guyon's canal, the lower trunk of the brachial plexus at the

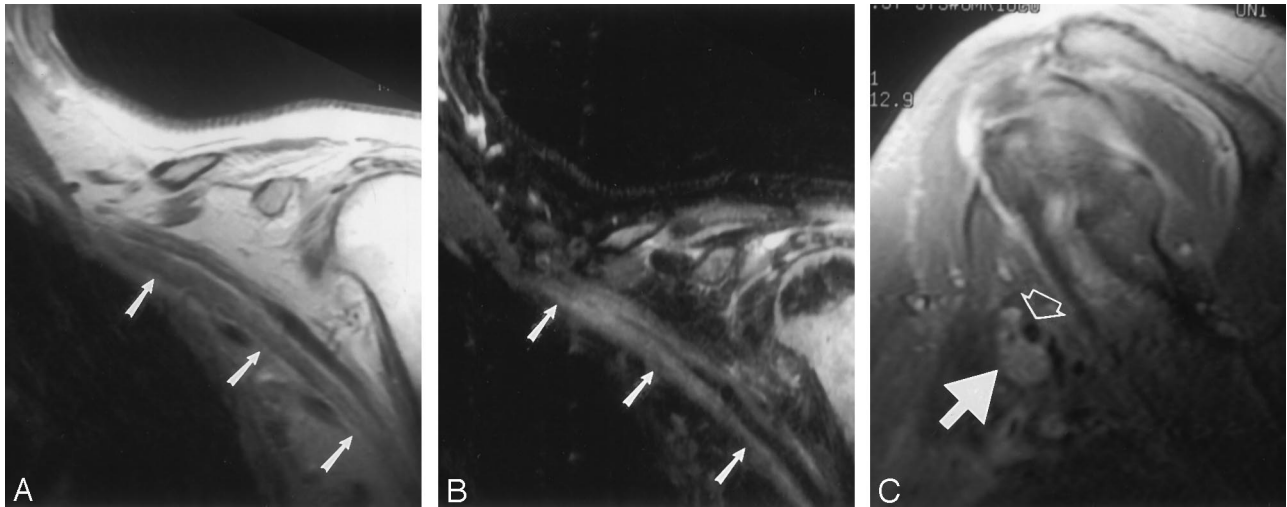


FIG 9. MR examination of the left brachial plexus in a patient who had had a mastectomy for breast cancer several years earlier and who presented with a new onset of symptoms of plexopathy in the left upper extremity. The differential diagnosis included recurrent tumor and radiation plexopathy.

A and B, Coronal T1-weighted (A) and STIR (B) images of the distal brachial plexus show marked diffuse enlargement of the medial cord of the brachial plexus (arrows).

C, Oblique sagittal fat-suppressed T1-weighted image at the level of the acromial clavicular joint shows the enlarged, contrast-enhancing medial cord (solid arrow). The position of the axillary artery is designated by the open arrow. Imaging appearance is that of diffuse tumor infiltration of the medial cord, which was proved by positron emission tomography and subsequent clinical follow-up.

insertion of the anterior scalene muscle on the first rib (scalenus anticus syndrome) or at the crossing of a cervical rib (cervical rib syndrome) (23), the sciatic nerve at the greater sciatic foramen (piriformis syndrome), and the lateral femoral cutaneous nerve near the attachment of the inguinal ligament to the anterior superior iliac spine (meralgia paresthetica) (7). Compressive neuropathy or plexopathy may also result from hematoma or aneurysmal formation in certain locations: iliopsoas hematoma causing femoral neuropathy or lumbar plexopathy, depending on the extent of hemorrhage, and aneurysm of the abdominal aorta, internal iliac, or gluteal arteries causing lumbosacral plexopathy. Currently, the presence of localized abnormal T2 signal of the involved nerve on MR images has been the most reliable finding and is useful to confirm the clinical diagnosis, to eliminate the possibility of a mass lesion, and to help with surgical planning and postsurgical follow-up.

Unexplained Neuropathy or Plexopathy

In cases in which the clinical examination does not reveal the cause of a neuropathy, MR imaging may identify a focal or diffuse nerve abnormality that may indicate a structural abnormality, such as may be seen with hereditary hypertrophic neuropathies (eg, Dejerine-Sottas disease) or an inflammatory pseudotumor of the nerve (24, 25) (Fig 7). Demonstration of a normal-appearing nerve is also useful because it narrows the differential diagnosis and may obviate interventional therapy. Not uncommonly, patients who undergo MR imaging for unexplained plexopathy will have idiopathic, probably postviral, inflammatory conditions, such as brachial or lumbosacral plexitis (neuritis).

Traumatic Nerve Injury

MR imaging is useful for examining patients in whom surgical intervention is being contemplated to repair nerve injury. Demonstration of the exact site and severity of injury is used to determine whether surgery is warranted and, if it is, to plan the surgical approach. Nerve injury can range from disruption of axonal conduction with preservation of anatomic continuity of all components comprising the nerve trunk (neurapraxic injury) to complete loss of continuity of the nerve trunk (severed nerve) with a neurotmetic injury (26, 27) (Fig 10). By depicting the morphology of the injured nerve, MR imaging complements electrophysiological studies to help determine the exact site and type of nerve injury and the potential for surgical treatment (Fig 11). In addition, it can show the relationship of the intact nerve to posttraumatic lesions, such as spindle, lateral, and stump neuromas, as well as focal or diffuse perineural fibrosis.

Posttreatment Evaluation

After surgical or medical treatment for peripheral neuropathy, MR imaging may show resolution of abnormal imaging findings, such as T2 hyperintensity and nerve swelling, weeks or months before there is clinical evidence of functional recovery (28) (Fig 12). Patients with a history of cancer and clinical signs of plexopathy after radiation therapy may have recurrent tumor or radiation-induced plexopathy. Imaging features that favor postradiation injury of the brachial plexus are abnormal swelling and increased T2 hyperintensity of the brachial plexus on the side of involvement. The increased size and signal intensity abnormalities diffusely and uniformly involve the plexus nerves within the radiation field (Fig 13). The absence

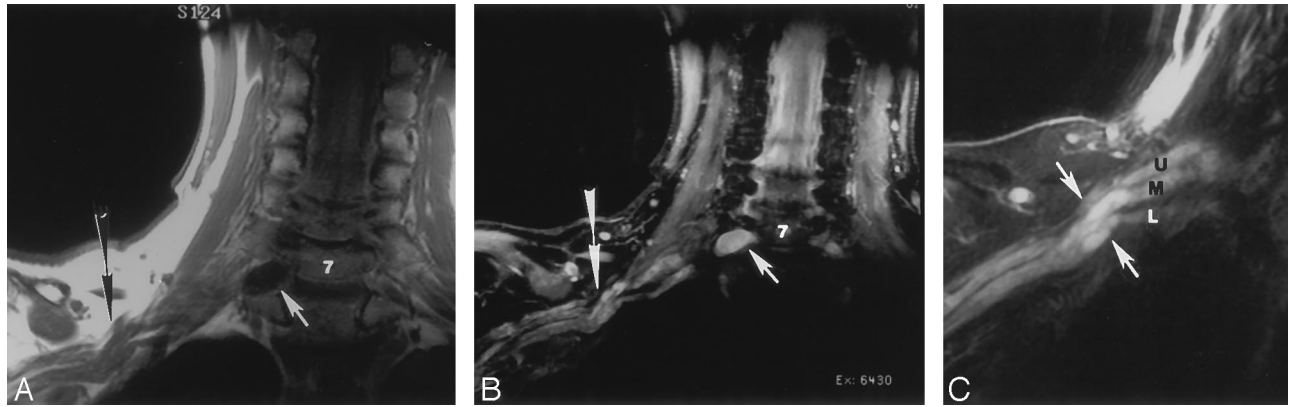
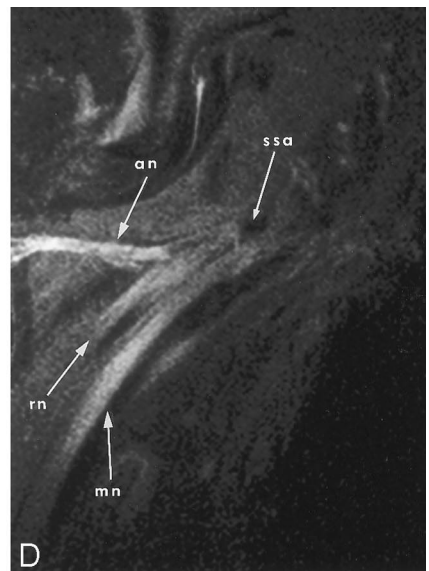
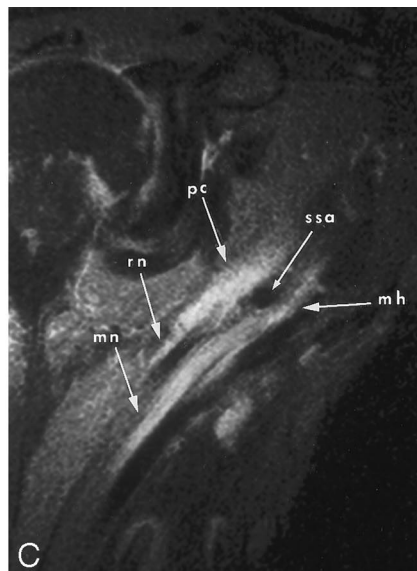
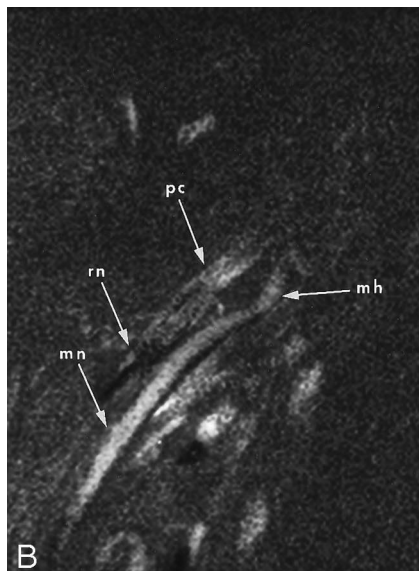
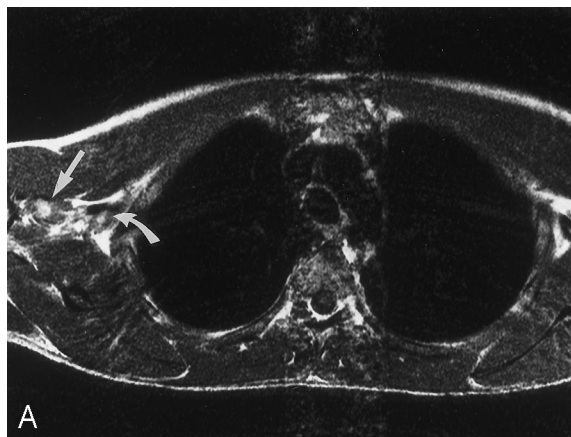


FIG 10. MR imaging of the right brachial plexus in a patient several weeks after injury to the right arm and shoulder in a motorcycle accident. A and B, Coronal T1-weighted (A) and fast spin-echo T2-weighted (B) images show a pseudomeningocele at the site of complete avulsion of the right C8 nerve root (*short arrow*). Also note marked deformity and localized hyperintense T2 signal due to severe stretch and compressive injury of the brachial plexus more distally at the level of the brachial plexus divisions and proximal cords (*long arrow*), resulting from fracture and inferior displacement of the clavicle. C, Reformatted T2-weighted image in an oblique plane along the length of the divisions of the brachial plexus trunks and the proximal cords shows the area of injury at the midclavicle level, with abnormally increased T2 signal intensity and deformity (*arrows*), to better advantage. The upper (U), middle (M), and lower (L) trunks of the brachial plexus are also identified.

FIG 11. Brachial plexus stretch injury in a 20-year-old man who reported severe pain in right shoulder and arm after a 7-hour operation (abdominal perineal resection) for recurrent rectal cancer. The pain persisted for 5 to 6 weeks then steadily decreased.

A, Axial contrast-enhanced T1-weighted MR image (obtained with a body RF coil as receiver) 2 weeks after surgery shows enhancement in the region of the coracobrachialis and biceps brachii muscles (*straight arrow*) as well as focal enhancement around the axillary vessels (*curved arrow*). These findings initially raised concern for possible metastatic disease.

B-D, A coronal T2-weighted fast spin-echo image (B) and contrast-enhanced fat-saturated T1-weighted spin-echo images (C and D) were subsequently obtained with a localized surface coil receiver 2 weeks later. B and C are corresponding sections, while D is located 3.5 mm posterior to C. Diffuse increased T2 signal (B) and contrast enhancement (C and D) involve the posterior cord (pc), the axillary (an) and radial (rn) nerves, as well as the median nerve (mn) and its medial head (mh), which pass inferior to the subscapular branch (ssa) of the axillary artery. The long, uniform involvement of cords and several peripheral nerves, without eccentric masses, favors a diagnosis of stretch injury over neoplasia. Nerve conduction studies and electromyography (EMG) done at the time of the second MR study confirmed involvement of the musculocutaneous, the radial, and, most severely, the median nerves. The ulnar nerve EMG was normal, whereas the axillary nerve was not assessed.



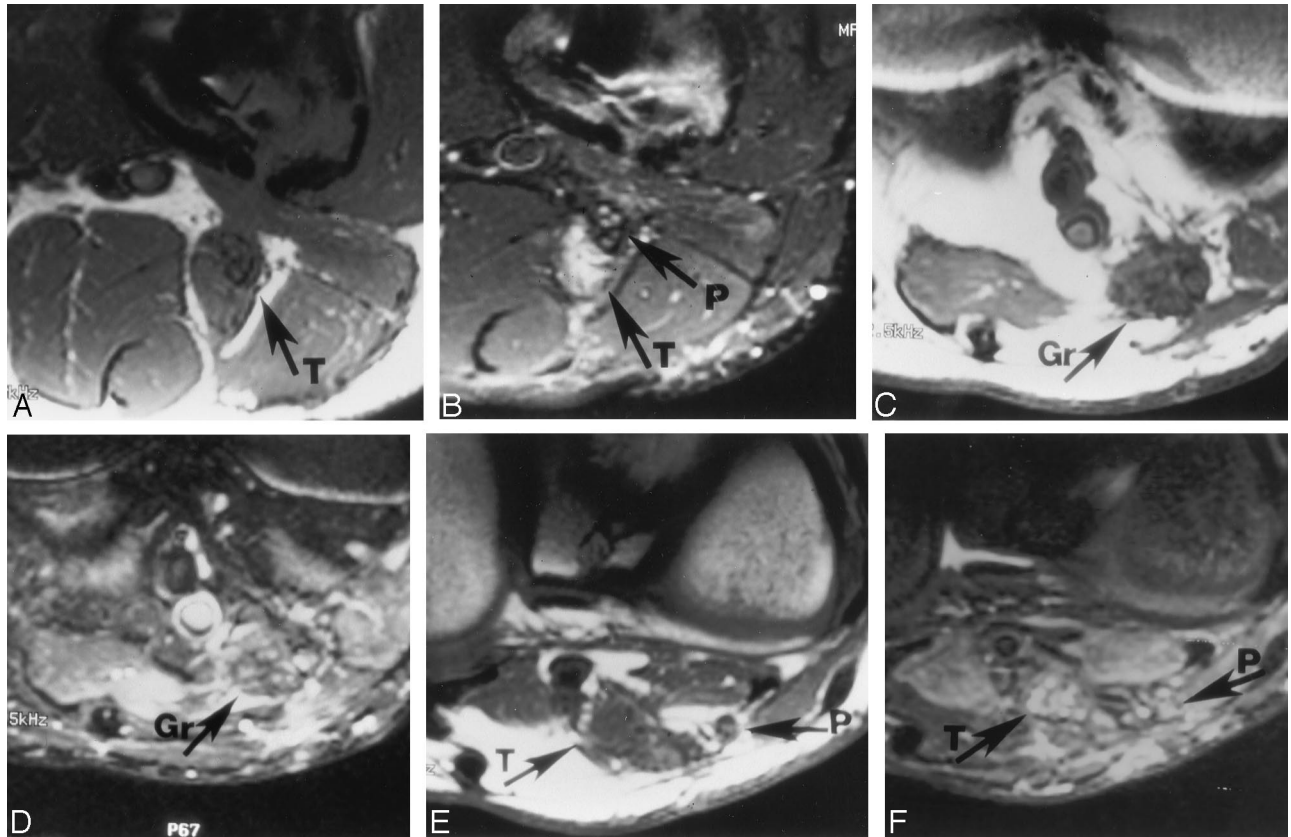


FIG 12. Patient with laceration in the popliteal fossa region resulting in transection injury of the tibial nerve, which was treated by means of a nerve graft bridging the site of nerve transection. MR imaging was done approximately 2 months after surgical repair.

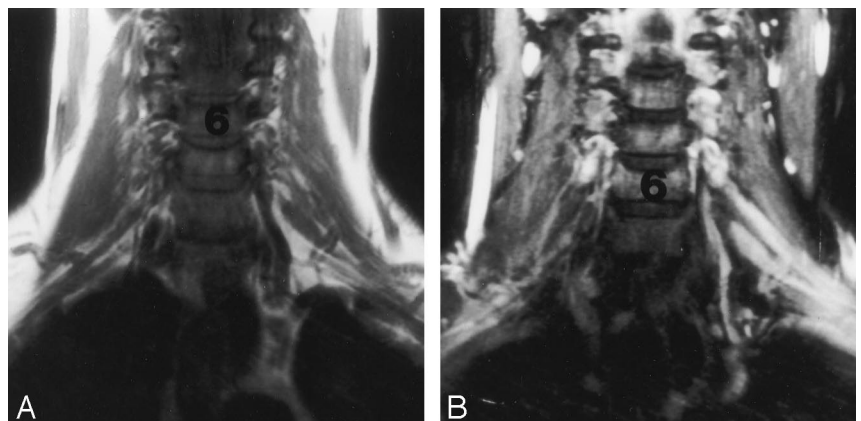
A and B, Axial T1-weighted (A) and STIR (B) images just proximal to the site of the graft show localized deformity and scarring surrounding the tibial and peroneal nerves, best seen on A. The tibial (T) and peroneal (P) branches of the sciatic nerve are visible. Note markedly hyperintense T2 signal within the injured tibial nerve just proximal to the graft. There is mild enlargement and some hyperintense fascicles within the peroneal branch as well, probably reflecting slight injury to this nerve and/or changes resulting from the previous surgery.

C and D, T1-weighted (C) and STIR (D) images at the level of the nerve graft (Gr). Hyperintense signal, resulting from postsurgical scarring, surrounds the area of the nerve graft on the STIR image. No recognizable fascicular structure is identified within the graft.

E and F, T1-weighted (E) and STIR (F) images at the level of the knee, just below the nerve graft site, again show scarring and deformity in the region of the tibial nerve stemming from postoperative changes after the previous injury. Abnormal hyperintense swollen fascicles are also identified within the distal tibial nerve (T). In our experience, this persistent hyperintense pattern is seen before axonal regrowth and return of function. In several cases that we have followed, the hyperintense signal appears to decrease with nerve regeneration and has preceded functional recovery to a variable degree. The distal common peroneal nerve (P) is also identified. The hyperintense signal within this nerve may represent changes related to the surgery and postoperative scarring.

FIG 13. Patient with signs and symptoms of progressive left brachial plexopathy 2 years after radiation to the left supraclavicular region and axilla for treatment of breast carcinoma. Differential diagnosis included recurrent tumor and radiation plexitis.

A and B, Coronal T1-weighted (A) and STIR (B) images of the brachial plexus on both sides show enlargement of the roots, trunks, and divisions of the brachial plexus on the left side. Note uniform and diffuse involvement of all visualized components of the left brachial plexus within the radiation field. Also note the marked difference in size and signal intensity of the structures of the left brachial plexus as compared with the right side. The findings in this case contrast sharply with those in Figure 9, of a patient with a similar clinical history and presentation but with focal enlargement of only a single cord of the brachial plexus. By comparison, the diffuse distribution of changes throughout all the neural structures within the radiation field distinguishes this case of brachial plexopathy from that of recurrent tumor infiltration in Figure 9, in which a single cord was enlarged with sparing of the adjacent neural structures.



of a focal or eccentric mass distinguishes radiation plexopathy from recurrent tumor (29). One should be aware, however, that radiation fibrosis often results in increased rather than decreased signal intensity within and around the nerves on T2-weighted images, and it can show postcontrast enhancement (30).

Current Limitations of MR Imaging of the Nerves

The most common causes of poor-quality images of peripheral nerves are inhomogeneous fat suppression, motion artifacts, and poor SNR due to inadequate RF coils. The variability of fat suppression depends on which region of the body is imaged and which technique is used. Variability is greatest on images of the brachial plexus in the shoulder region, because of the change in the size of the body parts between the neck and shoulders and because of the large amount of air present within the lungs and along the surface of the neck and shoulders—factors that affect magnetic susceptibility. The STIR technique is less sensitive to these factors than is the frequency-selective method and therefore is more likely to provide uniform fat suppression. For postcontrast T1-weighted acquisitions, frequency-selective fat saturation rather than STIR sequences must be used. Newer fat-suppression techniques have recently been developed, and these may prove more robust than the currently used methods (31, 32).

As is the case for most MR studies, motion artifacts generally result from two sources. The first is patient movement, usually due to the patient's inability to hold still for a long examination. This is especially problematic when studying nerves within the upper extremity, since it may be necessary to put the arm in a difficult or uncomfortable position in order to obtain optimal images. The second source is physiological motion due to respiration, cardiac pulsation, or blood flow. Phase-shift artifacts resulting from misregistered signal or from incompletely suppressed signal from intravascular flowing blood are propagated along the phase-encoded direction. These can cause significant degradation of T2-weighted images. While the artifacts can be reduced by suppressing the blood flow signal with spatially localized saturation pulses outside the FOV, the saturation pulses are often less effective in reducing artifacts from vessels with slowly flowing blood, such as small veins. The deleterious effects of flow artifacts can sometimes be avoided by interchanging the phase- and frequency-encoding gradient axes. Postcontrast T1-weighted images may also have prominent flow-related artifacts, owing to the shortened T1 relaxation time of gadolinium-containing blood. The intensity of flow-related artifacts is reduced on both T1- and T2-weighted sequences through a combination of gradient moment-nulled motion compensation and spatially localized RF flow-suppression pulses.

The availability of adequate phased-array coils is limited, particularly for evaluating the brachial plexus and for imaging certain peripheral nerves within the extrem-

ities. This problem will be overcome as manufacturers develop optimized coil designs that better address the imaging difficulties in specific areas of the body.

Conclusion

The preliminary results of high-resolution MR imaging presented here are promising. They show that individual normal nerves can be imaged, and that features of intraneural topography can be displayed. The morphology and signal intensity characteristics that distinguish abnormal from normal nerves are depicted; however, the accuracy, sensitivity, and clinical utility of these findings remain to be established. Potentially, additional morphologic findings, such as fascicle/nerve area ratios (7) or alterations in physical properties, such as water diffusion, will also help to characterize peripheral nerves and improve diagnostic specificity and sensitivity.

Advances in peripheral nerve imaging will of course depend on further improvements in RF coil technology and pulse sequence design that allow higher-quality T1- and T2-weighted images to be obtained in shorter scan times. Improvements in pulse sequence design may also make possible the application of physiological or functional imaging techniques. Diffusion-weighted imaging, for example, has been shown to depict subtle abnormalities within white matter tracts of the brain due to loss or reduction of diffusion anisotropy and to changes in diffusion along the axons. This method has also been applied to peripheral nerve imaging in an animal model, and feasibility has been demonstrated (33). It is anticipated that abnormalities may be detectable along the axons within peripheral nerves; however, their depiction in human subjects is complicated by the small size of peripheral nerves and by the susceptibility artifacts noted earlier. Finally, increased SNR can be achieved by imaging at higher field strengths. With the use of specialized RF transmitter and receiver coils, it may be feasible to image the peripheral nerves within the extremities at 3.0 to 4.0 T without exceeding the limit for RF-generated heat deposition within the whole body.

Acknowledgments

We thank Betsy Munk and Patricia Garland for their assistance in manuscript preparation and Paul Schwartz and Janet Schuker for their help with photography. Pradip Pattany and Greg Weaver provided technical advice and assistance, and Mary Bunge critically reviewed the discussion of peripheral nerve anatomy.

References

1. Bowen B. **Brachial plexus.** In: Bradley WG, Stark DD, ed. *Magnetic Resonance Imaging*. 3rd ed. Philadelphia: Mosby-Year Book; 1998:3 (in press)
2. Bowen B. **Lumbosacral plexus.** In: Bradley WG, Stark DD, ed. *Magnetic Resonance Imaging*. 3rd ed. Philadelphia: Mosby-Year Book; 1998:3 (in press)

3. Britz G, West G, Dailey A, et al. **Magnetic resonance imaging in evaluating and treating peripheral nerve problems.** *Perspect Neurol Surg* 1995;6:53-66
4. Filler A, Kliot M, Howe F, et al. **Application of magnetic resonance neurography in the evaluation of patients with peripheral nerve pathology.** *J Neurosurg* 1996;85:299-309
5. Aagaard B, Maravilla K, Kliot M. **MR neurography: MR imaging of peripheral nerves.** *Magn Reson Imaging Clin N Am* 1998;6:179-194
6. Fawcett D. In: Bloom and Fawcett, eds. *A Textbook of Histology*. 12th ed. New York: Chapman & Hall; 1994:336-339
7. Sunderland S. In: *Nerves and Nerve Injuries*. Baltimore: Williams & Wilkins; 1968:25-57, 733-1112
8. Ikeda K, Houghton V, Ho K-C, Nowicki B. **Correlative MR-anatomic study of the median nerve.** *AJR Am J Roentgenol* 1996;167:1233-1236
9. Kuntz C, Blake L, Britz G, et al. **Magnetic resonance neurography of peripheral nerve lesions in the lower extremity.** *Neurosurgery* 1996;39:750-756
10. Roemer P, Edelstein W, Hayes C, et al. **The NMR phased array.** *Magn Reson Med* 1990;16:192-225
11. Hayes C, Hattes N, Roemer P. **Volume imaging with MR phased arrays.** *Magn Reson Med* 1991;18:309-319
12. Hayes C, Tsuruda J, Mathis C, Maravilla K, Kliot M, Filler A. **Brachial plexus: MR imaging with a dedicated phased array of surface coils.** *Radiology* 1997;203:286-289
13. Cox I, Dillon W. **Low-cost device for avoiding bulk susceptibility artifacts in chemical-selective fat saturation MR of the head and neck.** *AJNR Am J Neuroradiol* 1995;16:1367-1369
14. Polak J, Jolesz F, Adams D. **Magnetic resonance imaging of skeletal muscle: prolongation of T1 and T2 subsequent to denervation.** *Invest Radiol* 1988;23:365-369
15. Fleckenstein J, Watumull D, Conner K, et al. **Denervated human skeletal muscle: MR imaging evaluation.** *Radiology* 1993;187:213-218
16. West G, Haynor D, Goodkin R, et al. **Magnetic resonance imaging signal changes in denervated muscles after peripheral nerve injury.** *Neurosurgery* 1994;35:1077-1086
17. Britz G, Haynor D, Kuntz C, Goodkin R, Gitter A, Kliot M. **Carpal tunnel syndrome: correlation of magnetic resonance imaging, electrodiagnostic, and intraoperative findings.** *Neurosurgery* 1995;37:1097-1103
18. Britz G, Haynor D, Kuntz C, et al. **Ulnar nerve entrapment at the elbow: correlation of magnetic resonance imaging, clinical, electrodiagnostic, and intraoperative findings.** *Neurosurgery* 1996;38:458-465
19. Dailey A, Tsuruda J, Goodkin R, et al. **Magnetic resonance neurography for cervical radiculopathy: a preliminary report.** *Neurosurgery* 1996;38:488-492
20. Beltran J, Rosenberg Z. **Diagnosis of compressive and entrapment neuropathies of the upper extremity: value of MR imaging.** *AJR Am J Roentgenol* 1994;163:525-531
21. Middleton W, Kneeland J, Kellman G, et al. **MR imaging of the carpal tunnel: normal anatomy and preliminary findings in the carpal tunnel syndrome.** *AJR Am J Roentgenol* 1987;148:307-316
22. Rosenberg Z, Beltran J, Cheung Y, Ro S, Green S, Lenzo S. **The elbow: MR features of nerve disorders.** *Radiology* 1993;188:235-240
23. Panegyres P, Moore N, Gibson R, Rushworth G, Donaghy M. **Thoracic outlet syndromes and magnetic resonance imaging.** *Brain* 1993;116:823-841
24. Tachi N, Kozuka N, Ohya K, Chiba S, Naganuma M. **MRI of peripheral nerves and pathology of sural nerves in hereditary motor and sensory neuropathy type III.** *Neuroradiology* 1995;37:496-499
25. Weiland T, Scheithauer B, Rock M, Sargent J. **Inflammatory pseudotumor of nerve.** *Am J Surg Pathol* 1996;20:1212-1218
26. Seddon H. **Three types of nerve injury.** *Brain* 1943;66:238-283
27. Sunderland S. **A classification of peripheral nerve injuries producing loss of function.** *Brain* 1951;74:491-516
28. Dailey A, Tsuruda J, Filler A, Maravilla K, Goodkin R, Kliot M. **Magnetic resonance neurography of peripheral nerve degeneration and regeneration.** *Lancet* 1997;350:1221-1222
29. Thyagarajan D, Cascino T, Harms G. **Magnetic resonance imaging in brachial plexopathy of cancer.** *Neurology* 1995;45:421-427
30. Bowen B, Verma A, Brandon A, et al. **Radiation-induced brachial plexopathy: MR and clinical findings.** *AJNR Am J Neuroradiol* 1996;17:1932-1936
31. Szumowski J, Coshov W, Li F, et al. **Double-echo three-point Dixon method for fat suppression MRI.** *Magn Reson Med* 1995;34:120-124
32. Xiang Q-S, An L. **Water-fat imaging with direct phase encoding.** *J Magn Reson Imaging* 1997;7:1002-1015
33. Howe F, Filler A, Bill B, Griffiths J. **Magnetic resonance neurography.** *Magn Reson Med* 1992;28:328-338

Please see the Editorial on page 1001 in this issue.